Since January 2020 Elsevier has created a COVID-19 resource centre with free information in English and Mandarin on the novel coronavirus COVID-19. The COVID-19 resource centre is hosted on Elsevier Connect, the company's public news and information website.

Biosensors and Bioelectronics 210 (2022) 114293

Contents lists available at ScienceDirect

Biosensors and Bioelectronics

journal homepage: www.elsevier.com/locate/bios

Rotational diffusometric sensor with isothermal amplification for ultra-sensitive and rapid detection of SARS-CoV-2 *nsp2* cDNA

Dhrubajyoti Das [a], Cheng-Wen Lin [b,c], Jae-Sung Kwon [d,**], Han-Sheng Chuang [a,e,f,*]

[a] Department of Biomedical Engineering, National Cheng Kung University, Tainan, 701, Taiwan
[b] Department of Medical Laboratory Science and Biotechnology, China Medical University, Taichung, Taiwan
[c] Department of Medical Laboratory Science and Biotechnology, Asia University, Wufeng, Taichung 413, Taiwan
[d] Department of Mechanical Engineering, Incheon National University, Incheon, Republic of Korea
[e] Medical Device Innovation Center, National Cheng Kung University, Tainan, 701, Taiwan
[f] Core Facility Center, National Cheng Kung University, Tainan, 701, Taiwan

ARTICLE INFO

Keywords:
Rotational diffusometry
SARS-CoV-2 *nsp2* cDNA
Janus particle
Loop-mediated isothermal amplification
Real-time PCR
Open-well microfluidic chip

ABSTRACT

In the wake of a pandemic, the development of rapid, simple, and accurate molecular diagnostic tests can significantly aid in reducing the spread of infections. By combining particle imaging with molecular assays, a quick and highly sensitive biosensor can readily identify a pathogen at low concentrations. Here, we implement functionalized particle-enabled rotational diffusometry in combination with loop-mediated isothermal amplification for the rapid detection of the SARS-CoV-2 *nsp2* gene in the recombinant plasmid as a proof of concept for COVID-19 diagnostics. By analyzing the images of blinking signals generated by these modified particles, the change in micro-level viscosity due to nucleic acid amplification was measured. The high sensitivity of rotational diffusometry enabled facile detection within 10 min, with a limit of detection of 70 ag/μL and a sample volume of 2 μL. Tenfold higher detection sensitivity was observed for rotational diffusometry in comparison with real-time PCR. In addition, the system stability and the effect of temperature on rotational diffusometric measurements were studied and reported. These results demonstrated the utility of a rotational diffusometric platform for the rapid and sensitive detection of SARS-CoV-2 cDNA fragments.

1. Introduction

Facing an unprecedented pandemic threat, fast and sensitive molecular diagnostic tests play an important role in controlling the spread of infectious pathogens and enable early disease management. In molecular diagnosis, nucleic acid amplification tests (NAATs) deliver highly sensitive detection of extremely low-concentrated pathogens in the early stage of diseases, especially newly emerging and re-emerging infectious outbreaks (Innis et al., 1988; Sharafeldin and Davis, 2021; Yang and Rothman, 2004). Recently, COVID-19, caused by severe acute respiratory syndrome coronavirus 2 (SARS-CoV-2), has grown into a global pandemic and has become a serious health issue (Kevadiya et al., 2021). Numerous state-of-the-art techniques such as reverse transcriptase qualitative polymerase chain reaction (RT-qPCR) (Pan et al., 2020), clustered regularly interspaced short palindromic repeat (CRISPR) Cas12-based detection (Broughton et al., 2020; Zhang et al., 2022), enzyme-linked immunosorbent assay (ELISA) (Liu et al., 2021), electrochemical sensors (Kumar et al., 2022), plasmonic metasensors (Ahmadivand et al., 2021), and nanomaterial-based (Abdelhamid and Badr, 2021; Rasmi et al., 2021) POC devices have been developed in the past 2 years for the diagnosis of this fatal disease. Among these methods, nucleic acid amplification-based assays, specifically RT-qPCR, are considered the gold standard in research and clinical use because of their high accuracy. However, the complex thermal cycling process, expensive instrumentation, and laboratory setup hinder their exploitation for point-of-care (POC) diagnostics (Chang et al., 2017; Johnston et al., 2006; Li et al., 2019).

For this reason, isothermal nucleic acid amplification tests, collectively referred to iNAATs, have been employed to overcome the drawbacks of conventional PCR (Craw and Balachandran, 2012; Hai et al., 2020; Qi et al., 2018; Yue et al., 2021). The most common examples of such technologies include loop-mediated isothermal amplification

* Corresponding author. Department of Biomedical Engineering, National Cheng Kung University, Tainan, 701, Taiwan.
** Co-corresponding author. Department of Mechanical Engineering, Incheon National University, Incheon, Republic of Korea.
E-mail addresses: jsungkwon@inu.ac.kr (J.-S. Kwon), oswaldchuang@mail.ncku.edu.tw (H.-S. Chuang).

https://doi.org/10.1016/j.bios.2022.114293
Received 3 March 2022; Received in revised form 8 April 2022; Accepted 15 April 2022
Available online 20 April 2022

(LAMP) (Notomi, 2000), recombinase polymerase amplification (RPA) (Piepenburg et al., 2006), rolling circle amplification (RCA) (Yue et al., 2021), and nucleic acid sequence-based amplification (Zhao et al., 2015). Among the iNAATs, LAMP has been found as the most promising approach in both laboratory and POC diagnostics due to its large product formation (10^9–10^{10} copies) from very few target molecules in less than an hour (Notomi, 2000). Besides, LAMP has some added advantages in comparison with the other isothermal amplifications. For example, (1) LAMP does not require any complicated enzyme system like RPA, in which a DNA polymerase and single-stranded DNA binding proteins are required (Suea-Ngam et al., 2020). (2) In LAMP, three pairs of primers are used with six distinct target regions of the DNA sequence, making it highly specific compared with NASBA (Trinh et al., 2019). (3) LAMP can be achieved with a single step reaction, whereas one additional ligation step is required before amplification for RCA (Kang et al., 2020; Yue et al., 2021).

Reverse transcriptase LAMP (RT-LAMP) screening emerged as an alternative molecular diagnostics test for COVID-19 by targeting several regions of the viral genome, including the spike protein gene (S gene), nucleocapsid protein gene (N gene), and RNA-dependent RNA polymerase gene (RdRp gene) (Carter et al., 2021; Davidson et al., 2021; Ganguli et al., 2021; Pang et al., 2020; Thompson and Lei, 2020). For example, STOPCovid is a CRISPR-integrated RT-LAMP-based one-pot process for the detection of COVID-19 with a limit of detection (LOD) of 100 copies/reaction in 70 min (Joung et al., 2020). Additionally, Yu et al. (2020) developed an isothermal LAMP-based method for the fluorometric detection of SARS-CoV-2 (iLACO) with a sensitivity of 10 copies/μL in 40 min. LAMP is not a novel approach only for viral diagnosis as it has been a familiar tool in bacterial studies. In past decades, a considerable number of LAMP assays have been established for the rapid detection of food and waterborne pathogens like *Escherichia coli* at a range of 48–100 CFU/mL in 25–35 min (Naik et al., 2019; Nguyen and Lee, 2021; Safavieh et al., 2012; Trinh et al., 2019), *Staphylococcus aureus* at 10 CFU/mL in 27 min (Srimongkol et al., 2020), *Salmonella typhi* at 23 CFU/mL (Duarte-Guevara et al., 2016), and *Enterococcus faecalis* at 130 copies/reaction in 45 min (Martzy et al., 2017). Meanwhile, LAMP integrated with a microfluidic and paper-based chip composed of polymethyl methacrylate and poly-dimethylsiloxane was demonstrated for improved feasibility of POC diagnostics (Huang et al., 2020; Zhang et al., 2019). Sayad et al. (2016) designed a disc-based LAMP chip for the detection of *Salmonella* with an LOD of 5 pg/μL. A cellulose-based paper microchip in combination with LAMP was developed by Roy et al. (2017) for the colorimetric detection of *Bacillus subtilis* with a sensitivity of 10 pg/μL. These reports displayed that LAMP is a potential method for the detecting a wide range of pathogens and biomolecular species with high accuracy and sensitivity.

Numerous methods have been developed for LAMP readout, where gel electrophoresis is the most popular technique due to its easy operation process. However, this method is time-consuming (Gadkar et al., 2018). To overcome such limitations, other strategies have been developed, including colorimetric detection using dyes like SYBR Green I or EvaGreen (Parida et al., 2005), pH analysis (Toumazou et al., 2013), and electrochemical methods by the addition of metal ion indicators, such as hydroxy naphthol blue dye and calcein/Mn^{2+} (Goto et al., 2009). Above all, fluorescent dyes, which display high sensitivity and tolerance toward proteins, are used extensively in the detection of LAMP (Francois et al., 2011). A major disadvantage that restricts the use of fluorescent dyes is the demand for high-tech instrumentation, as well as the reliance on detection techniques on relative estimations for adjusting the variation between repeats (Cao et al., 2017; Ocenar et al., 2019; Oscorbin et al., 2016; Rolando et al., 2019). In the case of pH and electrochemical sensing, the amplification results cannot be monitored without any use of power sources and additional indicators (Tanner et al., 2015).

Integration of LAMP with particle imaging can surpass the use of additional dyes and indicators by maximizing the robustness of LAMP and the high sensitivity of particle imaging. LAMP generates a large number of nucleic acid targets, that eventually change the solution viscosity (Clayton et al., 2017, 2019; Moehling et al., 2020). This micro-level viscosity change can be quantified using an optical detection technique called rotational diffusometry, enabled by functionalized Janus particles (Chen et al., 2019; Das et al., 2021). These half fluorescents and half gold particles produce a significant blinking signal under a fluorescent microscope (Fig. 1). Images of these blinking particles are captured through a charge-coupled device (CCD) camera and analyzed by a cross-correlation algorithm (Chen and Chuang, 2020). According to the Stokes–Einstein–Debye relation, the rotational diffusion of microscopic particles is inversely proportional to the fluid viscosity (Cruickshank Miller, 1924; Debye, 1929). Therefore, in the presence of positive LAMP, the increased viscosity will result in a decrease in diffusivity and particle rotation. Conversely, in the case of negative LAMP, solution viscosity stays constant. Thus, the diffusivity of Janus particles remains stable. In our previous proof of concept work, we successfully demonstrated that rotational diffusometry combined with LAMP can be employed to detect *E. coli* with an LOD of 42.8 fg/μL in less than 10 min (Das et al., 2022).

On the basis of our previous achievements in diffusometric techniques (Cheng and Chuang, 2019; Chuang et al., 2018; Wang et al., 2018, 2019, 2020; Yang et al., 2020), we propose a rapid, specific, and sensitive detection of SARS-CoV-2 cDNA fragment in the recombinant plasmid as a proof of concept for COVID-19 diagnosis (Fig. 1). The plasmid was synthesized by incorporating the *nsp2* gene of the SARS-CoV-2 viral genome into an available vector. To the best of our knowledge, this work is the first to attempt detection at a high level of speed and sensitivity of in vitro SARS-CoV-2 cDNA using rotational Brownian motion in combination with LAMP. Through this biosensing method, an LOD of 70 ag/μL was achieved in only 10 min. Compared with conventional PCR, the developed method has been proven to be 10-fold more sensitive and 12-fold faster. Overall, rotational diffusometry pairing with LAMP provides insight into the ultra-fast and sensitive detection of infectious pathogens. Thus, by incorporating reverse transcriptase LAMP (RT-LAMP), we envision integrating this technology into a microfluidic chip for POC diagnostics of COVID-19 in a timely fashion.

2. Material and methods

2.1. Construction, growth, and extraction of pET-32a-nsp2 plasmid

RNA was extracted from the SARS-CoV-2 virus using a commercial RNA extraction kit, and the amount was quantified using a microspectrophotometer. The complementary DNA of the *nsp2* gene from the viral RNA was synthesized using a commercially available transcription kit. The synthesized cDNA was inserted into pET-32a (+) vector (Novagen) by the T_4 DNA ligase (Thermofisher Scientific) at the *Nde*I and *Xho*I sites to construct the recombinant pET-32a (+)-*nsp2* plasmid and transformed into *E. coli* (Fig. 2). Bacterial cultures containing the recombinant plasmids were stored in frozen stocks (5 mL of TS broth and 20% glycerol with 100 μL/mL ampicillin) and used for growing the bacterial culture (37 °C for 24 h). Gene Spin miniprep plasmid extraction kit (PT-MP530XL-V3, Pro-Tech Chemicals, Taiwan) was used to extract and purify the recombinant plasmid from the prepared culture and then determined using a micro-volume UV–vis spectrophotometer (One Drop Touch Pro, Biometrics Technologies, USA). The purified plasmids were serially diluted in molecular grade water and served as a template for PCR and LAMP reactions.

2.2. Bacterial culture and gDNA extraction

Frozen stocks of *S. aureus* (ATCC 23360), *E. coli* (ATCC 25922), and *Klebsiella pneumoniae* (ATCC 700603) were obtained from American Type Culture Collection (Manassas, VA, USA) and grown in TS broth at

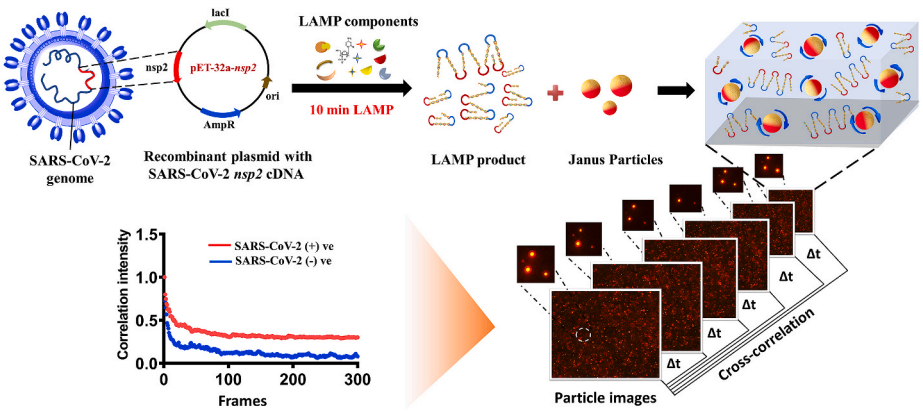

Fig. 1. Conceptual illustration of the experimental setup for the detection of SARS-CoV-2 using rotational diffusometry combined with LAMP. The recombinant plasmid containing the *nsp2* gene of SARS-CoV-2 virus was constructed. Amplification of these plasmids was performed by mixing the LAMP components and selected primers. The amplified nucleic acid was mixed with functionalized Janus microbeads. About 2 μL of the suspension was pipetted on the microchip setup and observed with a 10X objective lens under the IX71 microscope. The captured images were analyzed using a cross-correlation algorithm in MATLAB software.

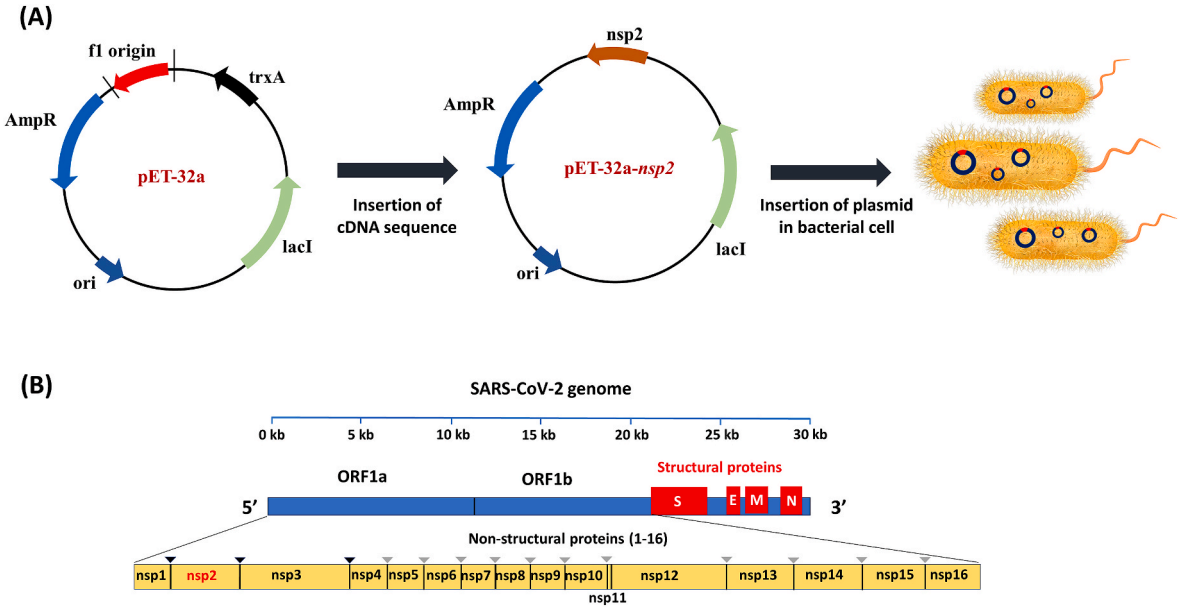

Fig. 2. (A) Construction of the pET-32a-*nsp2* plasmid. (B) SARS-CoV-2 genome structure.

37 °C for 24 h gDNA extraction and purification from these bacterial cultures (Gram-negative - *E. coli*, and *K. pneumoniae*; Gram-positive - *S. aureus*) were performed using a DNA extraction kit (PT-GD112, Pro-Tech chemicals, Taiwan) according to the manufacturer's instructions. The gDNA concentration of each bacterial strain was determined using a micro-volume UV–vis spectrophotometer, adjusted to the same concentration, and used as a template for LAMP reaction.

2.3. LAMP assay for SARS-CoV-2 nsp2 cDNA

Six LAMP primers (Table S1), namely, a pair of inner (FIP and BIP) and outer (F3 and B3) primers and two loop primers (LF and LB), were designed to target several district regions of the non-structural protein 2 (*nsp2*) of the *ORF1a* gene sequence of SARS-CoV-2 using Primer Explorer V5. Details of a single (25 μL) LAMP reaction (T100 thermal cycler, Bio-Rad, USA) are given in Table S2. All the LAMP amplifications were performed at 70 °C, confirmed by gel electrophoresis using 1.5% agarose gel at 100 V for 40 min, stained with a clear vision DNA stain (PT-D1001, Pro-Tech chemicals, Taiwan), and imaged via the BluView Transilluminator (MBE-300, Major Science, USA).

2.4. PCR and real-time PCR of SARS-CoV-2 nsp2 cDNA fragments

Conventional PCR (T100 thermal cycler, Bio-Rad, USA) and real-time PCR reactions (Step one plus system, Applied Biosystems) were performed with isolated plasmids using Fast-Run Taq Master Mix (PT-TMM228-D, Pro-Tech Chemicals, Taiwan) and Fast-start universal SYBR green master (rox) (4913914001, Roche, Germany), respectively. Primers with different amplicon sizes of 162 and 266 bp (Table S1) for the targeted gene *nsp2* of the SARS-CoV-2 genome were designed using PrimerQuest™ Tool. Details of single PCR and real-time PCR (20 μL) are provided in Tables S3 and S4, respectively. Real-time PCR included an initial denaturing step at 95 °C for 10 min, followed by 40 cycles of denaturation at 95 °C for 15 s, annealing, and extension at 60 °C for 60 s. A thermal denaturation protocol completed the process. Sequence Detection System (Applied Biosystems) software was used to determine the cycle threshold (C_T) values. All conventional PCR reactions strictly followed sequential steps: initial denaturation at 95 °C for 4 min, 30 thermal cycles of denaturation at 95 °C for 30 s, annealing at −55 °C for 40 s, extension at 72 °C for 40 s, and a final extension at 72 °C for 10 min.

2.5. Working principle of rotational Brownian motion in combination with LAMP

The microscopic particle in a suspension exhibits natural random movements, which is known as Brownian motion. According to the particle's rotation and vibration, this phenomenon can be classified into rotational and translational motion. Rotational Brownian motion is defined according to the Stokes–Einstein–Debye relation (Debye, 1929), which can be expressed as follows:

$$D_r = \frac{k_B T}{\pi \mu d_p^3}, \quad (1)$$

where T is temperature, μ is fluid dynamic viscosity, k_B is Boltzmann constant, and d_p is particle diameter. As mentioned in Equation (1), rotational diffusivity is inversely proportional to fluid viscosity and particle diameter and directly proportional to temperature when the two other variables are constant. Additionally, small particles provide a better signal than large particles, as the sedimentation due to gravity is low for the small particles.

LAMP amplifies the number of nucleic acid strands (10^9–10^{10} copies), which cause a change in microlevel viscosity resulting in a considerable difference in the diffusivity of the particles (Clayton et al., 2017, 2019; Moehling et al., 2020). In the presence of target nucleic acid, positive LAMP increases the sample viscosity, which decreases the rotational diffusion of the particles, resulting in the generation of slow blinking signals. However, the fluid viscosity remains unchanged if there is no target nucleic acid in the sample as it does not undergo the LAMP reaction. This contributes to a comparatively fast-blinking signal in comparison with the positive LAMP sample. This microlevel viscosity change due to nucleic acid amplification was investigated by the quantification of the blinking signal generated by functionalized Janus particles (half gold and half fluorescent) using a cross-correlation algorithm (Fig. 1). It involves capturing a series of images of microparticles undergoing rotational Brownian motion and calculating their correlation intensity of paired images concerning elapsed time. In this statistical method, the blinking signals of the particles are calculated in a given pair of images (I_1 and I_2) at times 0 and $0 + \Delta t$. All images are divided into four square grid regions known as interrogation windows for rapid calculation. The correlation intensity of each window is then added in the correlation domain. The correlation of these images with an increased time interval will result in cross-correlation intensity, which is identical to the cross-correlation function's peak value. Along with time, the correlation intensity peak value appears to decline because of the loss of pairs. A slow decrease in correlation intensity peak occurs due to weak diffusion of the particles. However, the intensity peak drops rapidly in the case of strong diffusion. The cross-correlation intensity diagram is normalized using the following exponential regression:

$$A \exp\left(-\frac{t}{\varnothing}\right) + B, \quad (2)$$

where $\varnothing$ is the characteristic correlation time of the intensity diagram, t is the elapsed time, and A and B are constants established through data fitting. The correlation time can be expressed as

$$\varnothing = \frac{\mu V}{k_B T}, \quad (3)$$

where V is the volume of the particles. Therefore, the correlation time is proportional to the fluid viscosity as the equivalent volume of microbead is fixed at a constant temperature.

2.6. Experimental rotational diffusometric measurements

Functionalized Janus particles (d = 1 μm) were thoroughly mixed with the LAMP product and dispersed uniformly in the solution through 20 s of sonication. A droplet of 2 μL of the LAMP-particle mixture was added on a hydrophobic glass slide, and a glass coverslip was placed on top of the sample with a spacer of 110 μm to create a sandwiched suspension. This coverslip limited the convective evaporation of the sample during the image capturing process, as sample evaporation contributed to changes in the microlevel viscosity. The sample was imaged at 25 °C using an inverted fluorescent microscope (Olympus, Tokyo, Japan) equipped with a 10× objective and a mercury lamp. Six measurements, of which 300 images constituted one measurement, were recorded for each sample by using a CCD camera at a frame rate of 10 Hz. The blinking signals generated from the Janus microparticles were analyzed with a cross-correlation algorithm, and the characteristic correlation times were plotted using MATLAB code.

3. Results and discussion

3.1. LAMP of SARS-CoV-2 nsp2 cDNA fragment and specificity of primers

The recombinant plasmids synthesized by incorporating the cDNA fragment of the SARS-CoV-2 *nsp2* gene into a pET-32a (+) vector were used in this study. The synthesized plasmids were initially analyzed with PCR where a clear band was observed for both 162 and 266 bp primers in 1.5% agarose gel electrophoresis (Fig. S1, supporting information). After a successful confirmation, the plasmid products were subjected to LAMP. The gel image showed a smear of multiple bands that authenticated the completed LAMP reaction (Fig. S2, supporting information).

Rotational diffusometric studies on the identification of LAMP were validated by incubating 1 μm functionalized Janus particles with the LAMP product. The Janus particles were prepared by coating 30 nm gold film on one side of the 1 μm fluorescent polystyrene particles using an e-beam evaporator (synthesis procedure is provided in the supporting information). As a result of the half gold and half fluorescent structure, these particles produced a blinking signal under fluorescent microscopy. Additionally, gold exhibited a strong SPR behavior as irradiated by green light (absorption peak 520–550 nm). This contributed to an improved LOD by enhancing the rotational Brownian motion (Chen and Chuang, 2020). The complete characterization of Janus particles and the working mechanism of rotational diffusometry were thoroughly explained in our previous work (Chen et al., 2019; Chen and Chuang, 2020). Six measurements were obtained for each sample by placing the sample-particle mixture droplets (2 μL) with a distance of 200 μm apart in the microchip setup while maintaining the temperature at 25 °C. About 2 μL of sample was used to provide a suitable sandwiched suspension and an ideal concentration of particles for image analysis. The blinking images of sampled microparticles were recorded with a CCD camera and further analyzed with a cross-correlation algorithm. Compared with the control, the sample containing LAMP-amplified SARS-CoV-2 *nsp2* cDNA fragments exhibited a relatively higher value in correlation time with a statistically significant difference ($p < 0.001$; Fig. 3A). Here, the control underwent a LAMP reaction containing no template plasmids. Moreover, a correlation intensity plot derived from Equation (2) showed a clear decline in the cross-correlation intensity with time. The decrease in the correlation intensity was observed due to the loss of pairs. Fig. 3B shows a rapid reduction in the correlation intensity for control; by contrast, in the case of the sample, a slow drop indicated the weak diffusion of the particles.

The specificity of the designed LAMP primers was tested with *E. coli, K. pneumoniae*, and *S. aureus* (Fig. 3C). No non-specific banding was distinguished in the gel image other than the desired plasmid, which indicated the specificity and selectivity of the designed primers. The specificity of primers was confirmed with rotational diffusometry (Fig. 3C). Meanwhile, no statistically significant difference was found for the control strains.

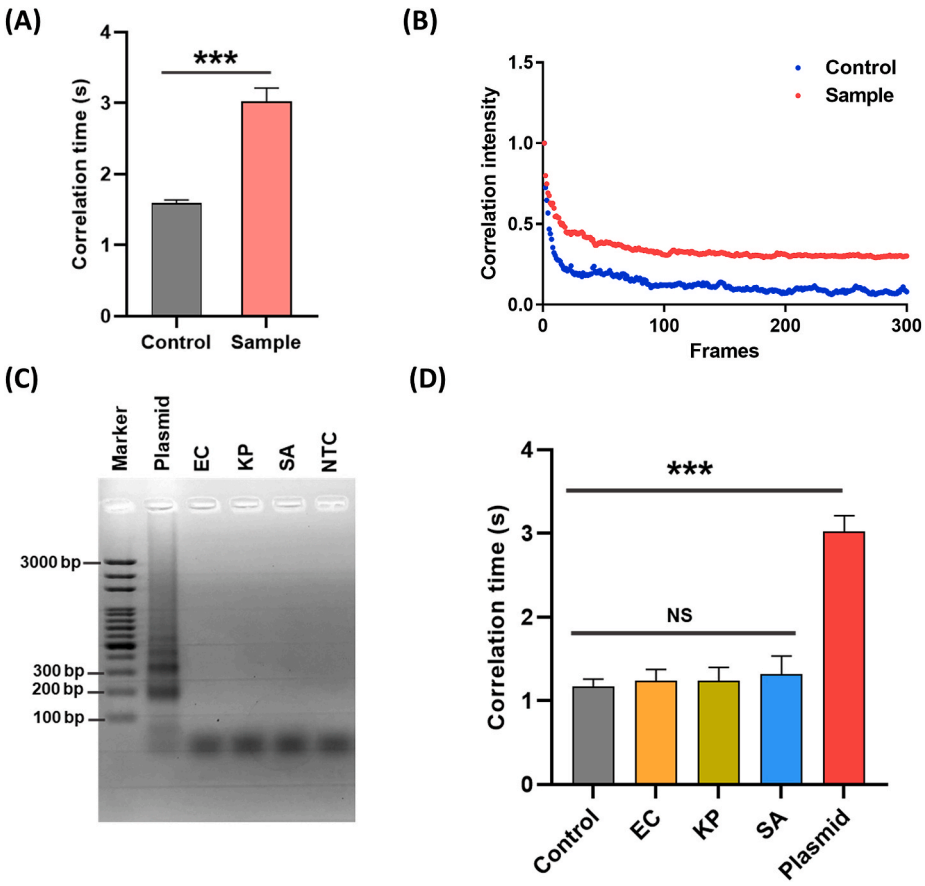

Fig. 3. (A) Correlation time of LAMP-amplified SARS-CoV-2 *nsp2* cDNA fragments (sample) in comparison with the control. The LAMP reaction was performed at 70 °C, and the control contained no template plasmids. (B) Correlation intensity of LAMP-amplified SARS-CoV-2 *nsp2* cDNA fragments (sample) in comparison with the control. The blue and red curves refer to the control and sample containing the plasmids, respectively. (C) LAMP amplicons of SARS-CoV-2 *nsp2* cDNA fragments and its specificity test with other control strains. (D) Change in correlation time of LAMP product targeting SARS-CoV-2 *nsp2* cDNA and a comparison with other control strains (KP, *K. pneumoniae*; EC, *E. coli*; SA, *S. aureus*) (***$p < 0.001$, $n \geq 3$).

3.2. Effect of LAMP reaction time

The effect of time on LAMP reaction of SARS-CoV-2 *nsp2* cDNA fragments was studied using the diffusometric method and gel electrophoresis within 5–40 min with a template plasmid concentration of 1 ng/μL. The gel electrophoresis image showed a gain in band intensity with time, indicating the rise in the amplified product (Fig. 4A). An anticipated increasing trend in correlation time was also noticed in the diffusometric measurements (Fig. 4B). A relatively statistically significant value ($p < 0.05$) between the sample that underwent LAMP for 5 min and the control confirmed the successful detection of SARS-CoV-2 *nsp2* cDNA in merely 5 min. These results demonstrated the rapidness of rotational diffusometry for nucleic acid amplification detection.

3.3. System stability

To understand the effect of external biomolecules on LAMP and diffusometric measurements, we conducted a series of experiments, where 2 μL of BSA solution with different concentrations viz. 0.1–10 μg/mL was added during the LAMP (Table S5). A constant concentration of

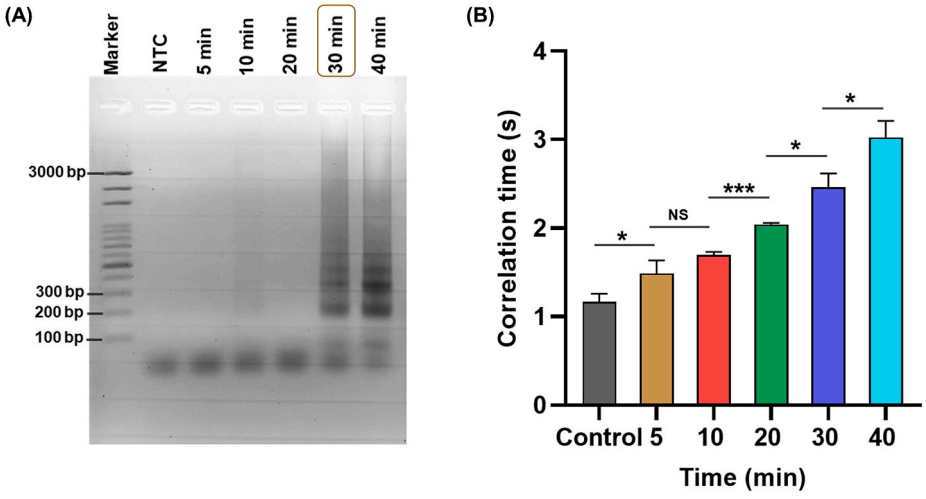

Fig. 4. (A) Gel electrophoresis of LAMP-amplified SARS-CoV-2 *nsp2* cDNA fragments in different reaction times. (B) Correlation time plot of LAMP-amplified SARS-CoV-2 *nsp2* cDNA for different reaction times. (*$p < 0.05$, ***$p < 0.001$, $n \geq 3$).

plasmid (1 ng/μL) was maintained, and a 40 min LAMP reaction was performed for all the experiments. Fig. 5A shows the successful detection of LAMP product within all the different concentrations of BSA with a relatively statistically significant difference (**$p < 0.01$, ***$p < 0.001$) from the control. An overall decreasing trend in correlation time suggested the reduction of LAMP product due to the interference of BSA. Gel electrophoresis was also performed to evaluate LAMP assay, in which the results showed good agreement with diffusometric data (Fig. S3). Furthermore, to investigate the effect of temperature on diffusometric measurements, a series of experiments was carried out by changing the microchip temperature from 15 °C to 35 °C during the image capture of the LAMP samples (plasmid concentration of 1 ng/μL and 40 min of LAMP; Fig. 5B). A decreasing trend in the correlation time was observed with an increase in temperature matching with the condition in Equation (3). These results exhibited a high tolerance and stability of LAMP reactions toward the presence of a large concentration of proteins in the sample, making this a robust method for the detection of pathogens in contaminated sample matrices.

3.4. Detection of SARS-CoV-2 by rotational diffusometry

LAMP targeting the *nsp2* gene was performed with a serially diluted plasmid solution with concentration ranging from 1 pg/μL to 0.1 fg/μL. All dilutions were amplified with a 10 min LAMP reaction. The viscosity changes in these LAMP products were identified by rotational diffusometry (Fig. 6A). Data showed a rising trend in correlation time with the increase in initial plasmid concentrations. Thus, high amplification resulted in a large viscosity change. Products of these LAMP assays showed a statistically significant difference among the control and the sample dilutions of 0.1 fg/μL ($p < 0.01$) for rotational diffusometry (single sample repeats in Fig. S5). The LOD was eventually estimated to be 70 ag/μL, which followed a three-sigma rule (defined as the intersection of the trend line of the concentration and the three standard deviations of the control; Fig. S4, supporting information). Amplifications were also confirmed by gel electrophoresis, showing banding up to 100 fg/μL for a 40 min LAMP reaction (Fig. 6B). Our findings were validated and compared with real-time and conventional PCR (Fig. 6C and D), and the resulting data were in good agreement with the diffusometric assay. Fig. 6C demonstrated a rapid amplification of *nsp2* cDNA fragments with high initial concentrations in real-time PCR. The detection sensitivity of 1 fg/μL was achieved for real-time PCR with a C_T value of 31.2, resulting in a total analysis time of 120 min. This result indicated a 10-magnitude improvement in detection sensitivity and a 12-fold improvement in detection time by the proposed method (analysis time: 10 min) in comparison with real-time PCR. Conventional PCR was performed with 266 bp primer pair (Table S1). The gel electrophoresis image showed banding up to 10 fg/μL dilution with 30 thermal cycles (analysis time: 150 min; Fig. 6D), making rotational diffusometry 100-fold higher in sensitivity and 15-fold faster than conventional PCR. In comparison with conventional PCR, LAMP produces a very high number of polymerized DNA chains in a very short period. Thus, ultrafast and sensitive detection of SARS-CoV-2 plasmids was achieved with rotational diffusometric sensors combined with LAMP. The sensitivity and rapidness of the diffusometric sensor were compared with other existing methods in the literature for SARS-CoV-2 detection (Table S6). Notably, the time mentioned for this study in Table S6 is composed of nucleic acid amplification (10 min) and detection time (5 min). This result suggested that LAMP-combined rotational diffusometry is a robust and rapid technique for nucleic acid amplification-based detection of pathogens with excellent sensitivity.

4. Conclusion

In this work, we demonstrated a rotational diffusometric sensor combined with LAMP for the ultra-fast detection of SARS-CoV-2 *nsp2* cDNA fragments with high sensitivity as a proof of concept for COVID-19 diagnosis. The plasmid was prepared by incorporating the *nsp2* gene segment of the SARS-CoV-2 genome into a pET-32a (+) vector and transformed into *E. coli* cells. The presence of the desired gene in the plasmid was confirmed by PCR and LAMP reactions. By using rotational diffusometry, we achieved an LOD of 70 ag/μL in 10 min with a sample volume of 2 μL. This method was 10-fold more sensitive and 12-fold more rapid than real-time PCR. Additionally, our assay facilitated high stability in the presence of external protein interference. Altogether, these results demonstrated that rotational Brownian motion is an ultrasensitive, fast, and robust method for revolutionizing the nucleic acid amplification-based detection of SARS-CoV-2 cDNA fragments. In the future, we envision bringing the entire process inside a microfluidic chip to develop a fully integrated LAMP-on-chip platform for rapid, sensitive, and real-time POC diagnostics of infectious pathogens, including COVID-19.

CRediT authorship contribution statement

Dhrubajyoti Das: Conceptualization, Investigation, Methodology, Data curation, Formal analysis, Writing – original draft, Writing – review & editing. **Cheng-Wen Lin:** Investigation, Methodology, Writing – review & editing. **Jae-Sung Kwon:** Project administration, Supervision, Funding acquisition, Writing – review & editing. **Han-Sheng Chuang:** Conceptualization, Project administration, Supervision, Funding acquisition, Writing – original draft, Writing – review & editing.

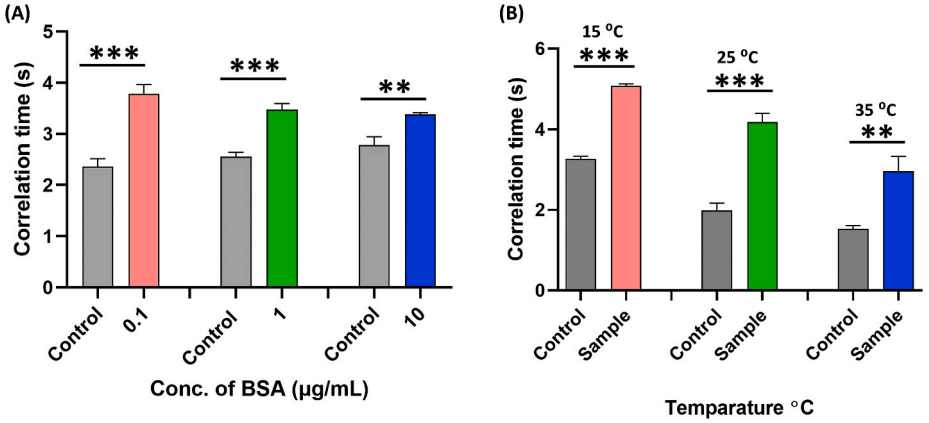

Fig. 5. (A) Effect of the presence of external protein (BSA) on the LAMP reaction of SARS-CoV-2 *nsp2* cDNA fragments. (B) Effect of temperature on diffusometric measurements of the LAMP samples (**$p < 0.01$, ***$p < 0.001$, $n \geq 3$).

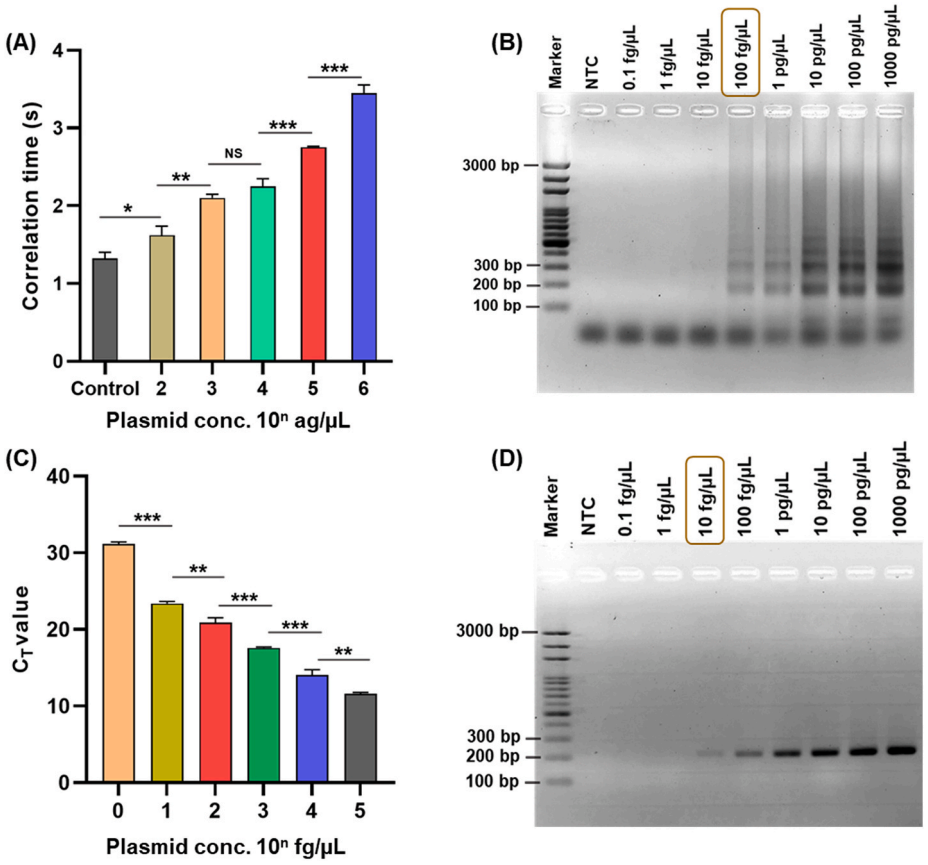

Fig. 6. (A) Correlation time of 10 min LAMP with different plasmid concentrations. (B) Gel electrophoresis of 40 min LAMP with different plasmid concentrations. (C) C_T value of real-time PCR with different plasmid concentrations. (D) A 1.5% agarose gel electrophoresis of PCR amplicons in different dilutions. (**p < 0.01, ***p < 0.001, n ≥ 3).

Declaration of competing interest

The authors declare that they have no known competing financial interests or personal relationships that could have appeared to influence the work reported in this paper.

Acknowledgments

This work was supported by Incheon National University (International Cooperative) Research Grant in 2021.

Appendix A. Supplementary data

Supplementary data to this article can be found online at https://doi.org/10.1016/j.bios.2022.114293.

References

Abdelhamid, H.N., Badr, G., 2021. Nanotechnol. Environ. Eng. 6, 1–26.
Ahmadivand, A., Gerislioglu, B., Ramezani, Z., Kaushik, A., Manickam, P., Ghoreishi, S. A., 2021. Biosens. Bioelectron. 177, 112971.
Broughton, J.P., Deng, X., Yu, G., Fasching, C.L., Servellita, V., Singh, J., Miao, X., Streithorst, J.A., Granados, A., Sotomayor-Gonzalez, A., Zorn, K., Gopez, A., Hsu, E., Gu, W., Miller, S., Pan, C.Y., Guevara, H., Wadford, D.A., Chen, J.S., Chiu, C.Y., 2020. Nat. Biotechnol. 38, 870–874.
Cao, Y., Wang, L., Duan, L., Li, J., Ma, J., Xie, S., Shi, L., Li, H., 2017. Sci. Rep. 7, 1–12.
Carter, J.G., Orueta Iturbe, L., Duprey, J.-L.H.A., Carter, I.R., Southern, C.D., Rana, M., Whalley, C.M., Bosworth, A., Beggs, A.D., Hicks, M.R., Tucker, J.H.R., Dafforn, T.R., 2021. Proc. Natl. Acad. Sci. Unit. States Am. 118.
Chang, D., Tram, K., Li, B., Feng, Q., Shen, Z., Lee, C.H., Salena, B.J., Li, Y., 2017. Sci. Rep. 7, 41598.
Chen, C.-J., Chen, W.-L., Phong, P.H., Chuang, H.-S., 2019. Sensors 19.
Chen, W.-L., Chuang, H.-S., 2020. Anal. Chem. 92, 12996–13003.
Cheng, H.-P., Chuang, H.-S., 2019. ACS Sens. 4, 1754–1760.
Chuang, H.-S., Chen, Y.-J., Cheng, H.-P., 2018. Biosens. Bioelectron. 101, 75–83.
Clayton, K.N., Berglund, G.D., Linnes, J.C., Kinzer-Ursem, T.L., Wereley, S.T., 2017. Anal. Chem. 89, 13334–13341.
Clayton, K.N., Moehling, T.J., Lee, D.H., Wereley, S.T., Linnes, J.C., Kinzer-Ursem, T.L., 2019. Sci. Rep. 9, 1739.
Craw, P., Balachandran, W., 2012. Lab Chip 12, 2469–2486.
Cruickshank Miller, C., 1924. Proc. R. Soc. London Ser. A 106, 724–749.
Das, D., Chen, W.L., Chuang, H.S., 2021. Anal. Chem. 93, 13945–13951.
Das, D., Hsieh, H.-C., Chen, C.-S., Chen, W.-L., Chuang, H.-S., 2022. Small Sci., 2200010
Davidson, J.L., Wang, J., Maruthamuthu, M.K., Dextre, A., Pascual-Garrigos, A., Mohan, S., Putikam, S.V.S., Osman, F.O.I., McChesney, D., Seville, J., Verma, M.S., 2021. Biosens. Bioelectron. 9, 100076.
Debye, P., 1929. Polar molecules. J. Soc. Chem. Ind. 48, 1036–1037.
Duarte-Guevara, C., Swaminathan, V.V., Reddy, B., Huang, J.-C., Liu, Y.-S., Bashir, R., 2016. RSC Adv. 6, 103872–103887.
Francois, P., Tangomo, M., Hibbs, J., Bonetti, E.-J., Boehme, C.C., Notomi, T., Perkins, M. D., Schrenzel, J., 2011. Med. Microbiol. 62, 41–48.
Gadkar, V.J., Goldfarb, D.M., Gantt, S., Tilley, P.A.G., 2018. Sci. Rep. 8, 5548.
Ganguli, A., Mostafa, A., Berger, J., Lim, J., Araud, E., Baek, J., de Ramirez, S.A., Baltaji, A., Roth, K., Aamir, M., Aedma, S., Mady, M., Mahajan, P., Sathe, S., Johnson, M., White, K., Kumar, J., Valera, E., Bashir, R., 2021. Anal. Chem. 93, 7797–7807.
Goto, M., Honda, E., Ogura, A., Nomoto, A., Hanaki, K.-I., 2009. Biotechniques 46, 167–172.
Hai, X., Li, Y., Zhu, C., Song, W., Cao, J., Bi, S., 2020. TrAC - Trends Anal. Chem. 133, 116098.
Huang, T., Li, L., Liu, X., Chen, Q., Fang, X., Kong, J., Draz, M.S., Cao, H., 2020. Anal. Methods 12, 5551–5561.
Innis, M.A., Myambo, K.B., Gelfand, D.H., Brow, M.A., 1988. Proc. Natl. Acad. Sci. Unit. States Am. 85, 9436–9440.
Johnston, S.P., Pieniazek, N.J., Xayavong, M.V., Slemenda, S.B., Wilkins, P.P., Da Silva, A.J., 2006. J. Clin. Microbiol. 44, 1087–1089.
Joung, J., Ladha, A., Saito, M., Segel, M., Bruneau, R., Huang, M.W., Kim, N.-G., Yu, X., Li, J., Walker, B.D., Greninger, A.L., Jerome, K.R., Gootenberg, J.S., Abudayyeh, O. O., Zhang, F., 2020. medRxiv. Preprint, 20091231.
Kang, Y.K., Im, S.H., Ryu, J.S., Lee, J., Chung, H.J., 2020. Biosens. Bioelectron. 168, 112566.
Kevadiya, B.D., Machhi, J., Herskovitz, J., Oleynikov, M.D., Blomberg, W.R., Bajwa, N., Soni, D., Das, S., Hasan, M., Patel, M., Senan, A.M., Gorantla, S., McMillan, J.E.,

Edagwa, B., Eisenberg, R., Gurumurthy, C.B., Reid, S.P.M., Punyadeera, C., Chang, L., Gendelman, H.E., 2021. Nat. Mater. 20, 593–605.
Kumar, N., Shetti, N.P., Jagannath, S., Aminabhavi, T.M., 2022. Chem. Eng. J. 430, 132966.
Li, H., Zhang, H., Xu, Y., Tureckova, A., Zahradník, P., Chang, H., Neuzil, P., 2019. Sensor. Actuator. B Chem. 283, 677–684.
Liu, Y., Tan, Y., Fu, Q., Lin, M., He, J., He, S., Yang, M., Chen, S., Zhou, J., 2021. Biosens. Bioelectron. 176, 112920.
Martzy, R., Kolm, C., Brunner, K., Mach, R.L., Krska, R., Šinkovec, H., Sommer, R., Farnleitner, A.H., Reischer, G.H., 2017. Water Res. 122, 62–69.
Moehling, T.J., Lee, D.H., Henderson, M.E., McDonald, M.K., Tsang, P.H., Kaakeh, S., Kim, E.S., Wereley, S.T., Kinzer-Ursem, T.L., Clayton, K.N., Linnes, J.C., 2020. Biosens. Bioelectron. 167, 112497.
Naik, P., Jaitpal, S., Shetty, P., Paul, D., 2019. Sensor. Actuator. B Chem. 291, 74–80.
Nguyen, H.A., Lee, N.Y., 2021. Biosens. Bioelectron. 189, 113353.
Notomi, T., 2000. Nucleic Acids Res. 28, e63.
Ocenar, J., Arizala, D., Boluk, G., Dhakal, U., Gunarathne, S., Paudel, S., Dobhal, S., Arif, M., 2019. PLoS One 14, 1–18.
Oscorbin, I.P., Belousova, E.A., Zakabunin, A.I., Boyarskikh, U.A., Filipenko, M.L., 2016. Biotechniques 61, 20–25.
Pan, Y., Zhang, D., Yang, P., Poon, L.L.M., Wang, Q., 2020. Lancet Infect. Dis. 20, 411–412.
Pang, B., Xu, J., Liu, Y., Peng, H., Feng, W., Cao, Y., Wu, J., Xiao, H., Pabbaraju, K., Tipples, G., Joyce, M.A., Saffran, H.A., Tyrrell, D.L., Zhang, H., Le, X.C., 2020. Anal. Chem. 92, 16204–16212.
Parida, M., Horioke, K., Ishida, H., Dash, P.K., Saxena, P., Jana, A.M., Islam, M.A., Inoue, S., Hosaka, N., Morita, K., 2005. J. Clin. Microbiol. 43, 2895–2903.
Piepenburg, O., Williams, C.H., Stemple, D.L., Armes, N.A., 2006. PLoS Biol. 4, e204.
Qi, H., Yue, S., Bi, S., Ding, C., Song, W., 2018. Biosens. Bioelectron. 110, 207–217.
Rasmi, Y., Saloua, K.S., Nemati, M., Choi, J.R., Rasmi, 1 Y., Saloua, K.S., 2021. Nanomaterials 11, 1–25.
Rolando, J.C., Jue, E., Schoepp, N.G., Ismagilov, R.F., 2019. Anal. Chem. 91, 1034–1042.
Roy, S., Mohd-Naim, N.F., Safavieh, M., Ahmed, M.U., 2017. ACS Sens. 2, 1713–1720.
Safavieh, M., Ahmed, M.U., Tolba, M., Zourob, M., 2012. Biosens. Bioelectron. 31, 523–528.
Sayad, A.A., Ibrahim, F., Uddin, S.M., Pei, K.X., Mohktar, M.S., Madou, M., Thong, K.L., 2016. Sensor. Actuator. B Chem. 227, 600–609.
Sharafeldin, M., Davis, J.J., 2021. Anal. Chem. 93, 184–197.
Srimongkol, G., Ditmangklo, B., Choopara, I., Thaniyavarn, J., Dean, D., Kokpol, S., Vilaivan, T., Somboonna, N., 2020. Sci. Rep. 10, 7768.
Suea-Ngam, A., Bezinge, L., Mateescu, B., Howes, P.D., deMello, A.J., Richards, D.A., 2020. ACS Sens. 5, 2701–2723.
Tanner, N.A., Zhang, Y., Evans, T.C., 2015. Biotechniques 58, 59–68.
Thompson, D., Lei, Y., 2020. Sensor. Actuator. Rep. 2, 100017.
Toumazou, C., Shepherd, L.M., Reed, S.C., Chen, G.I., Patel, A., Garner, D.M., Wang, C.-J. A., Ou, C.-P., Amin-Desai, K., Athanasiou, P., Bai, H., Brizido, I.M.Q., Caldwell, B., Coomber-Alford, D., Georgiou, P., Jordan, K.S., Joyce, J.C., La Mura, M., Morley, D., Sathyavruthan, S., Temelso, S., Thomas, R.E., Zhang, L., 2013. Nat. Methods 10, 641–646.
Trinh, K.T.L., Trinh, T.N.D., Lee, N.Y., 2019. Biosens. Bioelectron. 135, 120–128.
Wang, J.-C., Chi, S.-W., Shieh, D.-B., Chuang, H.-S., 2019. Sensor. Actuator. B Chem. 278, 140–146.
Wang, J.-C., Chi, S.-W., Yang, T.-H., Chuang, H.-S., 2018. ACS Sens. 3, 2182–2190.
Wang, J.-C., Tung, Y.-C., Ichiki, K., Sakamoto, H., Yang, T.-H., Suye, S., Chuang, H.-S., 2020. Biosens. Bioelectron. 148, 111817.
Yang, S., Rothman, R.E., 2004. Lancet Infect. Dis. 4, 337–348.
Yang, Y.-T., Wang, J.-C., Chuang, H.-S., 2020. Biosensors 10, 181.
Yu, L., Wu, S., Hao, X., Dong, X., Mao, L., Pelechano, V., Chen, W.-H., Yin, X., 2020. Clin. Chem. 66, 975–977.
Yue, S., Li, Y., Qiao, Z., Song, W., Bi, S., 2021. Trends Biotechnol. 39, 1160–1172.
Zhang, H., Xu, Y., Fohlerova, Z., Chang, H., Iliescu, C., Neuzil, P., 2019. TrAC Trends Anal. Chem. 113, 44–53.
Zhang, K., Fan, Z., Ding, Y., Xie, M., 2022. Chem. Eng. J. 429, 132472.
Zhao, Y., Chen, F., Li, Q., Wang, L., Fan, C., 2015. Chem. Rev. 115, 12491–12545.